Paint Degradation

DOI: 10.1002/anie.201305753

Nanoscale Investigation of the Degradation Mechanism of a Historical Chrome Yellow Paint by Quantitative Electron Energy Loss spectroscopy Mapping of Chromium Species**

Haiyan Tan, He Tian, Jo Verbeeck, Letizia Monico, Koen Janssens, and Gustaaf Van Tendeloo*

Since the 19th century, the industrial expansion stimulated the development of synthetic pathways to many new materials, including various pigments of the chrome yellow family ($PbCrO_4$, $PbCr_{1-x}S_xO_4$ $(0.1 \le x \le 0.8)$, $(1-x)PbCrO_4 \cdot x\,PbO$), cadmium yellow (CdS), emerald green ($Cu(C_2H_3O_2)_2 \cdot 3\,Cu(AsO_2)_2$), and viridian green ($Cr_2O_3 \cdot 2\,H_2O$).[1] Chrome yellows are often encountered in paintings from the end of 19th Century, such as in *Falling leaves (Les Alyscamps)* by van Gogh (1853–1890),[2,3] but also in works by Seurat (1859–1891)[4] and others. They are known to be sensitive towards darkening when exposed to sunlight.[5] However, in a recent study,[6] it was found that the speed of the alteration process of the lead chromate based yellow paints is influenced both by their chemical composition (in terms of sulfate amount) and crystalline structure (monoclinic and/or orthorhombic): a profound darkening was observed only for those compounds containing a sulfur-rich solid solution of $PbCr_{1-x}S_xO_4$ $(x \ge 0.5)$ and those in which this compound is mainly present in the orthorhombic crystalline form.[6] Since different forms of the chrome yellow pigments were found to be present in several paintings by van Gogh,[3] this could provide a possible explanation why only some of the areas painted with this class of pigments appear darkened today. In recent years, a growing interest in the conservation of these paintings has arisen. Understanding the alteration processes of the pigments is of key importance both to (re)assess/optimize the conditions in which works of art are stored and/or to allow selection of appropriate restoration treatments.[1,7]

In previous studies, artificial aging of lead chromate based compounds were performed through (a combination of) UV/Vis light, heat, contaminants,[5,8–10] and atmospheric gases (such as SO_2[10] or H_2S[11]). By means of X-ray absorption near-edge structure (XANES) measurements at the micrometer scale, we previously demonstrated that the alteration of chromium yellow is associated with the reduction of the original Cr^{VI} centers to Cr^{III}.[1,6] Recently, Casadio and Rose characterized painting materials used by Picasso through XRF nanoprobe measurements;[12] the same authors also studied zinc-potassium chromate compounds in a painting by Seurat.[7] However, almost no other studies have been carried out to investigate at the nanoscale level the exact nature of the progression of the alteration mechanism of chrome yellows; nevertheless such information could yield more detailed insights into the sequence of chemical transformations that drive the degradation process, thereby providing additional and/or complementary information with respect to the knowledge already acquired at the microscale level by synchrotron radiation-based XANES methods.[1,3,13]

Herein, advanced methods of quantitative scanning transmission electron microscopy (STEM) and electron energy loss spectroscopy (EELS) were employed to perform such a nanoscopic investigation on a sample of historical chrome yellow paint, dating back to the late 19th century that was already well characterized by means of XANES and other techniques.[1,3,6] The chemical and structural variations in this material were investigated before and after an artificial aging treatment with UVA/Vis light. A microscopic degradation model is proposed that serves to explain all the observed core–shell structures of the pigment particles.

The paint employed for this study was obtained from an oil-paint tube belonging to the Flemish Fauvist Rik Wouters (1882–1913). Artificial aging turns its original bright yellow color deep brown.[1,6] Prior to ageing, cross-sectional TEM samples ($3 \times 7 \times 0.1\ \mu m^3$) were prepared by means of a focused

[*] H. Tan,[+] H. Tian,[+] Prof. J. Verbeeck, Prof. G. Van Tendeloo
EMAT, University of Antwerp
Groenenborgerlaan 171, 2020 Antwerp (Belgium)
E-mail: he.tian@ua.ac.be
tianhe.mumu@gmail.com
H. Tan[+]
CEMES-CNRS, nMat group, University of Toulouse
BP 94347, 31055 Toulouse Cedex 4 (France)
L. Monico, Prof. K. Janssens
Department of Chemistry, University of Antwerp
Groenenborgerlaan 171, 2020 Antwerpen (Belgium)
L. Monico
Centre SMAArt, Department of Chemistry and CNR-ISTM, Universitá degli Studi di Perugia
Via Elce di Sotto 8, 06123 Perugia (Italy)
[+] These authors contributed equally to this work.

[**] The Qu-Ant-EM microscope was funded by the Hercules foundation of the Flemish Government. Funding from the European Research Council under the 7th Framework Program (FP7), ERC grant No. 246791—COUNTATOMS and ERC Starting Grant No. 278510 VORTEX is acknowledged. This work was partially funded by the European Union Council under the 7th Framework Program (FP7) grant No. NMP3-LA-2010-246102 IFOX and a GOA project "XANES meets ELNES" of the University of Antwerp. We acknowledge financial support from the European Union under the Seventh Framework Program under a contract for an Integrated Infrastructure Initiative (Reference No. 312483-ESTEEM2), from the SDD programme (S2-ART project) of the Belgian Federal Government, and from the ESRF (experiments EC-504 and EC-799 at beamline ID21). We are also indebted to Luuk van der Loeff for lending us the sample material..

Supporting information for this article is available on the WWW under http://dx.doi.org/10.1002/anie.201305753.

ion beam (FIB). The same region of the sample was investigated before and after aging in the electron microscope to study at the micro- to nanoscale level the changes induced during the artificial aging step, which is described in more detail in the Supporting Information.[14]

Figure 1 a shows a cross-sectional view, obtained by high-angle annular dark field (HAADF) STEM of the topmost 2–3 micrometers of the paint, freshly removed from the 100 year old paint tube; In this *Z*-contrast image, particles with a size distribution between 20 and 300 nm can be observed inside the oil-based binding matrix (linseed oil). A 3D EELS spectrum image (SI region) was acquired from the region indicated by a green rectangle. In some of the particles, the Cr signal (Cr-$L_{2,3}$ edge from 575 eV) is absent from the spectrum (see particle (1), Figure 1 b). A few particles show Cr enrichment on the surface (see particle (2), Figure 1 b) or in the center (see particle (3), Figure 1 b), thus suggesting the phase separation of the material into different core–shell structures. However, the phase-specific identification of the particles is not straightforward, because of the presence of both Cr and O in $PbCrO_4$ and Cr_2O_3 in this heterogeneous multiphase system. It is, therefore, difficult on the basis of elemental information alone to demonstrate the presence of, for example, Cr_2O_3 in particle (2).

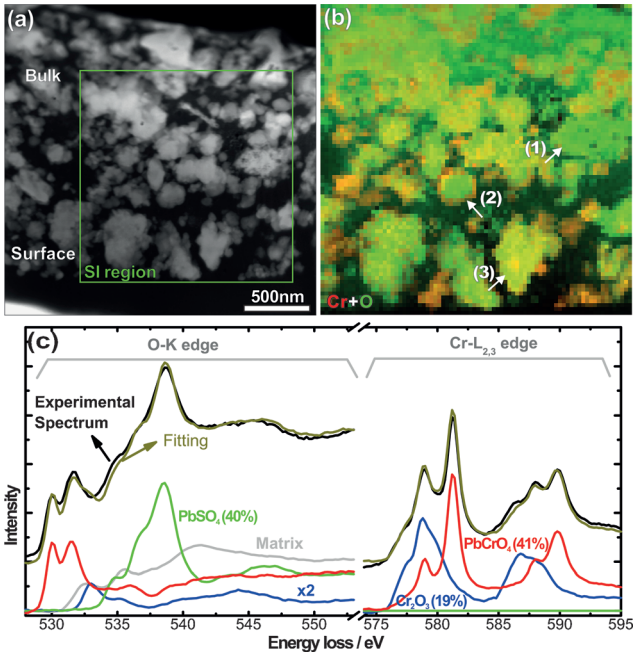

Figure 1. a) HAADF-STEM image of the historical pigment, indicating the region where the EELS investigation was carried out (SI region). b) Combined color map of the O (green) and Cr (red) elemental distribution mapped from the EELS K edge and $L_{2,3}$ edges in the region indicated by the green rectangle in (a). c) Experimental summed EELS spectrum (black, corresponding to a large sample area), and its fitted spectrum (olive) with multiple linear least squares fitting (MLLS) of the spectra of four components: $PbCrO_4$ (bulk), $PbSO_4$ (bulk), Cr_2O_3 (bulk), and matrix. The relative abundance of $PbSO_4$ (40%), $PbCrO_4$ (41%), and Cr_2O_3 (19%) in the total spectrum are indicated. The matrix spectrum consists mainly of a carbon K-edge (not shown) and a specific O-K edge. This matrix spectrum is used in the fitting procedure but its abundance mainly contains information about the density of particles and is, therefore, not relevant for the study of the chemical changes in the particles.

The energy-loss near-edge structure (ELNES) of the core-loss edges of the chemical elements is known to be sensitive to the chemical environment of the element in question.[15–18] Accordingly, the ELNES spectra from the $PbCrO_4$, $PbSO_4$, and Cr_2O_3 bulk reference materials all show a unique fingerprint and with significant differences at the O-K and Cr-$L_{2,3}$ edges (Figure 1 c; see the Supporting Information for more details).[14] The above references were chosen according to prior knowledge about the sample. Cr-K edge XANES measurements on the (un)aged paint yielded spectra that could be described well by a linear combination of the XANES spectra of $PbCrO_4$ and Cr_2O_3, while S-K edge XANES data confirmed the presence of different amounts of sulfur in the sulfate form.[1,3,6,13] The high-energy resolution of monochromated EELS (0.3 eV) enables the different phases in the sample to be identified on the basis of their ELNES fingerprints. This can be done in a much more selective manner than when simple elemental maps such as those of Figure 1 b are used for this purpose. A large set of EELS spectra, recorded when scanning the electron probe over the sample, (a so-called hyperspectral image) were fitted to a linear combination of these reference spectra and an averaged spectrum from the matrix. The resulting spectral weight maps represent the local abundance of each phase. The fitted spectra show a very satisfactory degree of similarity with the experimental spectra, thus providing a high confidence in this method and in the chosen references (Figure 1 c). The residual between the model and experiment shows no spectral or spatial features, thus indicating that the four reference components used here can adequately describe the spectra at the given noise level. Any further components are estimated to have a weight of less than 3% in terms of oxygen content for each spectrum in the dataset.

The spectral abundance maps of $PbCrO_4$, $PbSO_4$, and Cr_2O_3 (Figure 2) show their distribution at the nanometer scale in the examined area prior to aging. In general, the spectral signatures of $PbCrO_4$ and $PbSO_4$ are observed together, consistent with the presence of solid solution particles of $PbCr_{1-x}S_xO_4$. In addition, $PbSO_4$ can be observed as individual grains with a size of approximately 200 nm (particle (1) in Figure 2); it is also present on the surface of some particles. The Cr_2O_3 phase is mainly present as small particles or at the surface of some of the larger particles. Particle (2) clearly shows a $PbSO_4$–Cr_2O_3 core–shell structure. The $PbCrO_4$ phase is never observed to be present in a pure form but only as the core of core–shell structures with $PbSO_4$ and/or Cr_2O_3 at their surface. Particle (3) shows a three-layered $PbCrO_4$–$PbSO_4$–Cr_2O_3 core–shell structure. The insets in Figure 2 show more detailed maps of this particle. The layer thickness of both $PbSO_4$ and Cr_2O_3 are approximately 20 nm. The small surrounding satellite particles are mainly Cr_2O_3 with a very low amount of $PbCrO_4$ and $PbSO_4$. Spherical particle (4) shows a 10 nm Cr_2O_3 layer around a central $PbCrO_4$ core, while $PbSO_4$ is absent.

An ex situ experiment was conducted on this sample to evaluate the influence of UVA/Vis light on the same micrometer-sized region of this material. The results of the STEM-

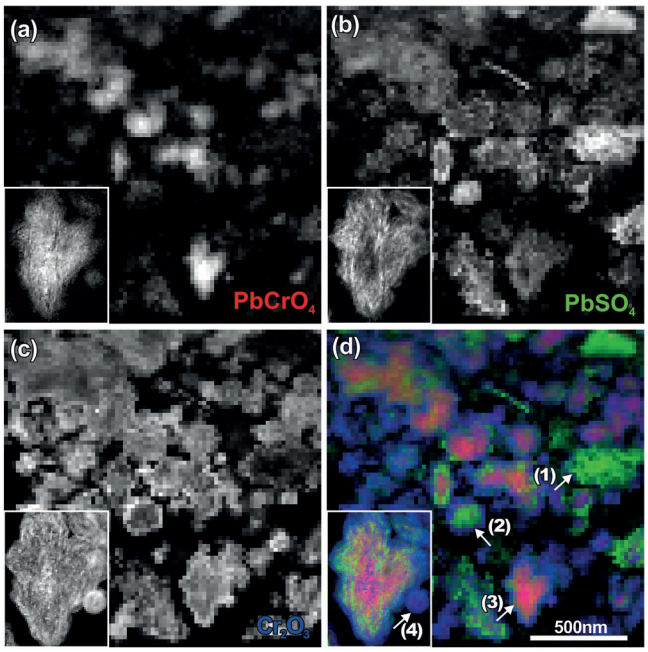

Figure 2. Spectral weight maps (phase maps) of $PbCrO_4$, $PbSO_4$, and Cr_2O_3 and their combined color map. The inset is an enlargement of particle (3), clearly showing a $PbCrO_4$–$PbSO_4$–Cr_2O_3 core–shell structure. The colors in (d) are scaled to the local maximum concentration of each phase in the imaging area.

EELS measurements, performed on the same area before and after 40 days of UVA/Vis aging treatment, are shown in Figure 3; it can be seen in the upper row images that the core–shell structures of some of the particles were already well-defined prior to artificial aging. The corresponding average phase composition comprises $(36\pm2)\%$ $PbCrO_4$, $(36\pm1)\%$ $PbSO_4$, and $(28\pm2)\%$ Cr_2O_3.

After aging, the $PbCrO_4$ concentration in the same area drops significantly to $(17\pm1)\%$ and the Cr_2O_3 content increases to $(46\pm1)\%$. These large changes in concentration indicate that the UVA/Vis treatment markedly accelerates the natural aging process; more than half of the $PbCrO_4$ in this area before the treatment was converted into Cr_2O_3. The phase images shown in Figure 3 indicate that most of the small $PbCrO_4$ particles have become completely reduced to Cr_2O_3 after aging, while a core of $PbCrO_4$ remains in the larger particles. Both the concentration and distribution of $PbSO_4$ remains the same before and after aging, thus indicating that either it is not involved at all in the degradation process or acts as a catalyst. Previous S-K edge XANES investigations of model paints[3,6], more recent Cr and S-K edge XANES and XRF analysis of a paint microsample taken from the painting *Falling leaves (Les Alyscamps)* by Van Gogh also support the latter view (see the Supporting Information for further details).

Based on the results shown here and those obtained by other techniques, such as XAS,[1,3,6,13] below we attempt to reconstruct the sequence of chemical transformations leading to the darkening of chrome yellow (Figure 4). Originally, we can assume that solid solution particles of pure $PbCrO_4$ (Figure 4a), pure $PbSO_4$ (Figure 4c), and $PbCr_{1-x}S_xO_4$ (Figure 4b) were present. During the 100 year period prior to the present experiments, some nanograins already spontaneously formed $PbCrO_4$–Cr_2O_3 and $PbCr_{1-x}S_xO_4$–$PbSO_4$ core–shell structures (Figure 4d,e).

As a first step of the transformation, CrO_4^{2-} ions (possibly in a partially protonated form, that is, as $HCrO_4^-$) are released by the $PbCr_{1-x}S_xO_4$ solid solution into microvolumes of moisture that are present in the voids between the pigment particles and the binding medium.[3,6] The greater the sulfate concentration of the solid solution and, therefore the degree to which the $PbCrO_4$ lattice is distorted, the greater is its solubility.[3] As a result of the high standard reduction potential of the $HCrO_4^-/Cr^{3+}$ redox couple ($E^0 = 1.21$ V, pH 1),[19] the solvated chromate ions can act as oxidants of other dissolved chemicals or of solid materials that are in contact with the aqueous solution, such as the organic matter, thereby giving rise to the formation of Cr_2O_3.[20,21] This insoluble Cr compound will precipitate out at all the available surfaces after the redox reaction. These surfaces include those of the $PbCrO_4$, $PbCr_{1-x}S_xO_4$, and $PbSO_4$ particles, thereby leading to particles with core–shell structures of the $PbCrO_4$–Cr_2O_3 (Figure 4d), $PbCrO_4$–$PbSO_4$–Cr_2O_3 (Figure 4h), and $PbSO_4$–Cr_2O_3 (Figure 4i) type. This transformation gradually depletes the cores of the Cr-containing nanograins so that the original $PbCrO_4$ particles (Figure 4a) may become Cr_2O_3 particles (Figure 4g); the depletion of the original $PbCr_{1-x}S_xO_4$ particles (Figure 4b) may advance to such an extent that only a $PbSO_4$ core remains, covered by an outer shell of precipitated Cr_2O_3 (Figure 4i). These four cases of core–shell structures have been observed in this experiment, while no other structures were present.

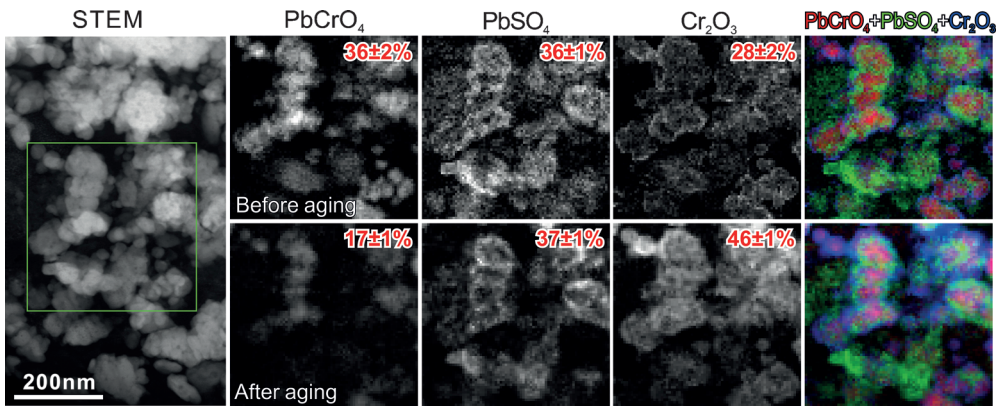

Figure 3. Ex situ comparison of the sample before and after aging under UVA/Vis light. A significant amount of $PbCrO_4$ was additionally reduced to Cr_2O_3 during the aging process. The systematic error is derived by inducting an experimental spectra variation of ±0.2 eV before fitting.

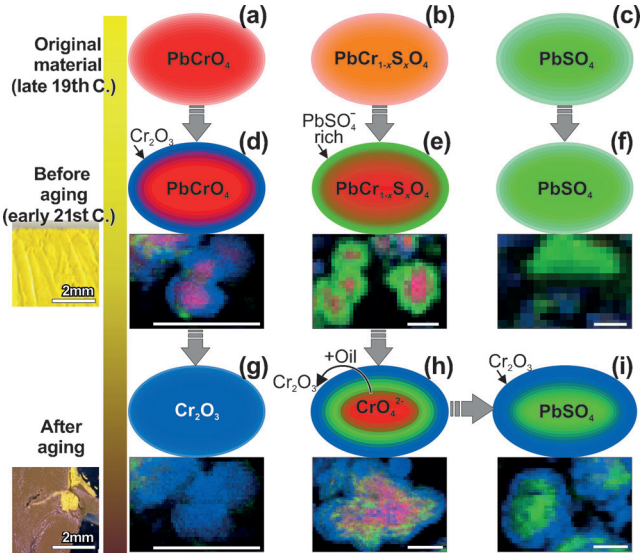

Figure 4. Proposed model of the degradation process of chromium yellow pigments. The original pigments in late 19th Century consisted of a) $PbCrO_4$, b) $PbCr_{1-x}S_xO_4$, and c) $PbSO_4$ particles. When the paint was taken out of the tube for investigation, the particles had gradually evolved to d) $PbCrO_4$–Cr_2O_3 core–shell, e) $PbCrO_4$–$PbSO_4$ core–shell, and remaining f) $PbSO_4$ particles, respectively. The subsequent artificial aging process speeds up the evolution and will lead them to g) Cr_2O_3, h) $PbCrO_4$–$PbSO_4$–Cr_2O_3, or i) $PbSO_4$–Cr_2O_3 core–shell structures. f) $PbSO_4$ particles will remain as a catalyst. All those intermediate or final states were observed in the experiment as shown in the bottom row. Scale bar: 100 nm.

The speed of the process may vary according to the size of the particles and their composition. Since $PbCrO_4$ and sulfur-poor $PbCr_{1-x}S_xO_4$ ($x<0.5$) are much more stable than the sulfur-rich $PbCr_{1-x}S_xO_4$ ($x>0.5$) solid solutions,[6] and thus release significantly less CrO_4^{2-} ions, the alteration affects them to a lesser extent. In our opinion, this supports the validity of the simple model based on the dissolution of chromate ions, a redox reaction at the interface between the solid material and the solution it is in contact with, followed by Cr_2O_3 precipitation (Figure 4) on the surface of the various particles present in the top layer of the paint.

In conclusion, to better identify the sequence of chemical reactions that are responsible for the degradation of historical chrome yellow pigments, a 100 year old chrome yellow paint sample was investigated down to the nanoscale, before and after artificial aging under UVA/Vis light. The O-K and Cr-$L_{2,3}$ core-loss edges were acquired in the STEM-EELS mode with high spatial and energy resolution. By comparing the subtle ELNES features in the spectra to those of references samples it was possible to visualize and quantify the phase distribution in two dimensions. Four types of core–shell particles could be identified from the phase maps in the sample. We propose a model in which $PbCrO_4$ degrades through dissolution of CrO_4^{2-} ions, which react with the organic binder of the paint at the interface with microdroplets of aqueous solution and after reduction precipitate as Cr_2O_3 at the surface of all present particles. This degradation model can explain all the observed core–shell particles observed.

Received: July 3, 2013
Published online: September 13, 2013

Keywords: analytical methods · chrome yellow · electron microscopy · reaction mechanisms · X-ray absorption spectroscopy

[1] L. Monico, G. Van der Snickt, K. Janssens, W. De Nolf, C. Miliani, J. Verbeeck, H. Tian, H. Tan, J. Dik, M. Radepont, M. Cotte, *Anal. Chem.* **2011**, *83*, 1214.
[2] E. Hendriks, L. Tilborgh, New views on Van Gogh's development in Antwerp and Paris: an integrated art historical and technical study of his paintings in the Van Gogh Museum, s.n., Amsterdam, **2006**.
[3] L. Monico, K. Janssens, C. Miliani, B. G. Brunetti, M. Vagnini, F. Vanmeert, G. Falkenberg, A. Abakumov, Y. Lu, H. Tian, J. Verbeeck, M. Radepont, M. Cotte, E. Hendriks, M. Geldof, L. van der Loeff, J. Salvant, M. Menu, *Anal. Chem.* **2013**, *85*, 851.
[4] J. Kirby, K. Stonor, A. Roy, A. Burnstock, R. Grout, R. White, *Natl. Gallery Tech. Bull.* **2003**, *28*, 437.
[5] R. J. Cole, *Paint Res. Assoc. Tech. Pap.* **1955**, *199*, 162.
[6] L. Monico, K. Janssens, C. Miliani, G. Van der Snickt, B. G. Brunetti, M. Cestelli Guidi, M. Radepont, M. Cotte, *Anal. Chem.* **2013**, *85*, 860.
[7] F. Casadio, S. Xie, S. Rukes, B. Myers, K. Gray, R. Warta, I. Fiedler, *Anal. Bioanal. Chem.* **2011**, *399*, 2909.
[8] V. Watson, H. F. J. Clay, *Oil Colour Chem. Assoc.* **1955**, *38*, 167177.
[9] A. Eibner, *Chem.-Ztg.* **1911**, *82*, 753755.
[10] L. J. H. Erkens, H. Hamers, R. J. M. Hermans, E. Claeys, M. Bijnens, *Surf. Coat. Int. Part B* **2001**, *84*, 1969.
[11] M. L. Somme-Dubru, M. Genet, A. Mathieux, P. G. Rouxhet, L. J. Rodrique, *Coat. Technol.* **1981**, *53*, 5156.
[12] F. Casadio, V. Rose, *Appl. Phys. A* **2013**, *111*, 1.
[13] L. Monico, G. Van der Snickt, K. Janssens, W. De Nolf, C. Miliani, J. Dik, M. Radepont, E. Hendriks, M. Geldof, M. Cotte, *Anal. Chem.* **2011**, *83*, 1224.
[14] Supporting Information.
[15] R. F. Egerton, *Electron Energy-Loss Spectroscopy in the Electron Microscope*, 3rd ed., Springer, New York, **2011**.
[16] L. Garvie, A. Craven, R. Brydson, *Am. Mineral.* **1994**, *79*, 411.
[17] H. Tan, S. Turner, E. Yücelen, J. Verbeeck, G. Van Tendeloo, *Phys. Rev. Lett.* **2011**, *107*, 107602.
[18] H. Tan, J. Verbeeck, A. Abakumov, G. Van Tendeloo, *Ultramicroscopy* **2012**, *116*, 24.
[19] J. Wang, K. Ashley, D. Marlow, E. C. England, G. Carlton, *Anal. Chem.* **1999**, *71*, 1027.
[20] F. A. Cotton, G. Wilkinson, C. A. Murillo, M. Bochmann, *Advanced Inorganic Chemistry*, Wiley Interscience, New York, **1999**.
[21] J. Kotaś, Z. Stasicka, *Environ. Pollut.* **2000**, *107*, 263.